



Article

Study of Electrodeposition and Properties of Composite Nickel Coatings Modified with $\text{Ti}_3\text{C}_2\text{T}_x$ MXene

Vitaly Tseluikin ^{1,*} , Asel Dzhumieva ² , Alena Tribis ¹, Denis Tikhonov ¹, Alexey Tsyganov ² , Nikolay Gorshkov ²  and Marina Lopukhova ¹

¹ Engels Technological Institute (Branch), Yuri Gagarin State Technical University of Saratov, 17 Svobody Square, 413100 Engels, Saratov Region, Russia; tribis2004@mail.ru (A.T.); tikhonov-denis@mail.ru (D.T.); mlopuhova@yandex.ru (M.L.)

² Department of Chemistry and Technology of Materials, Yuri Gagarin State Technical University of Saratov, 77 Polytechnicheskaya Street, 410054 Saratov, Saratov Region, Russia; aselka2796@gmail.com (A.D.); tsyganov.a.93@mail.ru (A.T.); gorshkov.sstu@gmail.com (N.G.)

* Correspondence: tseluikin@mail.ru

Abstract: In this work we have synthesized $\text{Ti}_3\text{C}_2\text{T}_x$ MXene powder and studied its structure. Composite electrochemical coatings (CECs) of Ni- $\text{Ti}_3\text{C}_2\text{T}_x$ MXene were obtained from a sulfate-chloride bath in the galvanostatic regime. The microstructure of CEC was researched using X-ray phase analysis and scanning electron microscopy methods. It has been established that a Ni- $\text{Ti}_3\text{C}_2\text{T}_x$ MXene CEC microhardness rises by about 1.80 times compared with electrolytic Ni without a dispersed phase. For corrosion research, different corrosive media is applied. The corrosion-electrochemical behavior of Ni- $\text{Ti}_3\text{C}_2\text{T}_x$ MXene CECs by the chronovoltamperometry method in 0.5 M H_2SO_4 solution has been investigated. Trials in 3.5% NaCl have shown that $\text{Ti}_3\text{C}_2\text{T}_x$ MXene inclusion into the matrix of the electrochemical Ni results in a decrease in the corrosion rate by 1.60–1.75 times. These effects are due to the addition of $\text{Ti}_3\text{C}_2\text{T}_x$ MXene into the nickel matrix and the formation of CECs with a strengthening fine-grained structure.

Keywords: composite electrochemical coatings; nickel; $\text{Ti}_3\text{C}_2\text{T}_x$ MXene; structure; microhardness; corrosion



Citation: Tseluikin, V.; Dzhumieva, A.; Tribis, A.; Tikhonov, D.; Tsyganov, A.; Gorshkov, N.; Lopukhova, M. Study of Electrodeposition and Properties of Composite Nickel Coatings Modified with $\text{Ti}_3\text{C}_2\text{T}_x$ MXene. *Coatings* **2023**, *13*, 1042. <https://doi.org/10.3390/coatings13061042>

Academic Editors: Shibo Li and JongHyeon Lee

Received: 12 May 2023

Revised: 30 May 2023

Accepted: 2 June 2023

Published: 4 June 2023



Copyright: © 2023 by the authors. Licensee MDPI, Basel, Switzerland. This article is an open access article distributed under the terms and conditions of the Creative Commons Attribution (CC BY) license (<https://creativecommons.org/licenses/by/4.0/>).

1. Introduction

The electrochemical deposition of nickel coatings is one of the most common methods for modifying the surface of metal products. Electrolytic nickel and the alloys based on it are superior to many metals in such properties as corrosion resistance, wear resistance, and hardness, which results in their wide application (gas and steam turbines, chemical and oil and gas equipment, medical instruments, etc.) [1,2]. By co-precipitating nickel with dispersed particles of various natures, it is possible to greatly improve its functional properties. Coatings obtained through the electrodeposition of metals together with the dispersed phase are called composite electrochemical coatings (CEC). In particular, nickel-based CECs are known for their excellent adhesion, good corrosion resistance, and abrasion resistance [2,3].

Compounds of various natures can be used as a dispersed phase in the deposition of nickel CECs. The modification of the nickel matrix with ceramic particles (SiC [4] TiO_2 [5]), polymers [6], and carbon compounds (fullerenes [7,8], carbon nanotubes [9–11], nanodiamonds [12], graphene, and its derivatives [13–15]) is known.

Recently, two-dimensional materials called MXenes, discovered in 2011, have aroused great interest [16–21]. MXenes are a new class of two-dimensional nanomaterials based on early transition metal carbides and/or nitrides and can be represented by a general formula $\text{M}_{m+1}\text{X}_m\text{T}_x$ ($m = 1\text{--}4$), where M is a transition metal (Sc, Ti, V, Cr, Nb, Ta, Nb, Zr,

or Mo), X–C and/or N, T_x –surface terminations (such as –O, –OH, –F, –Cl) [22]. The methods for obtaining MXenes are based on a selective etching of the A layer from $M_{n+1}AX_n$ (MAX) structures, where A is usually an element such as Al, Si, Ga, etc. However, Ti_3C_2 MXene is the most popular compound among these, due to its availability and unique set of functional properties. Etching is usually carried out by treating MAX phase powders in hydrofluoric acid (HF) or mixtures of hydrochloric acid (HCl) and fluoride salts (LiF, KF, etc.) [23]. The great interest in this class of nanomaterials is associated primarily with their exceptional optical, mechanical, electrical, magnetic, and physicochemical properties [24,25]. In this regard, MXenes are promising for a wide range of different applications, such as water treatment, energy storage, catalysts, sensors, and more [26]. In addition, due to the mechanical, tribological, and anti-corrosion properties of MXenes, they can be used in coatings to improve their anti-friction and anti-corrosion properties and to increase their microhardness. For example, their application as lubricating additives makes it possible to reduce the friction coefficient and improve their wear protection due to the formation of a layer from MXene nanosheets which has unique properties [27,28]. In Ref. [29], a polypyrrole/ $Ti_3C_2T_x$ coating was applied to stainless steel by galvanostatic electrodeposition. It has been shown that MXene plays a key role in improving corrosion resistance, anode protection, and adhesion. Currently, few studies have been published on the use of MXene in metal composite coatings to improve their properties. The authors of [30] show that the addition of $Ti_3C_2T_x$ and $Ti_3C_2T_x$ /MoS₂ particles into the composition of the Ni–P coating makes it possible to reduce the friction coefficient and increase the wear resistance, microhardness, etc. Similar results were obtained through the inclusion of $Ti_3C_2T_x$ –Ce into the Ni–P matrix [31], where, besides an increase in microhardness, corrosion resistance was also improved due to the effective blocking of the diffusion of aggressive substances. Furthermore, 2D MXene, especially $Ti_3C_2T_x$, has been widely used in the realm of corrosion inhibition and protective coatings [32].

However, there are practically no works on the modification of nickel with a $Ti_3C_2T_x$ MXene compound, so it is relevant to obtain composite nickel coatings containing $Ti_3C_2T_x$ MXene and to research the influence of this compound on the operating characteristics of electrolytic nickel.

The purpose of this study is to obtain Ni– $Ti_3C_2T_x$ MXene composite coatings in a stationary mode of electrolysis and to examine their structure and their physical–mechanical and corrosion properties.

2. Materials and Methods

(a) $Ti_3C_2T_x$ MXene synthesis

The Ti_3AlC_2 MAX phase precursor powder was obtained using the molten salt-assisted synthesis method [33] from TiC elemental powders (Mark B, TU 87 48-42-6-84, 0.8–1.5 μ m, Mreda, Beijing, China), Ti (PTM -1, TU 14-22-57-92, Polema, Tula, 88 Russia), and Al (PA 4, less 100 μ m, Russian Standard 6058-73, Nizhny Novgorod, Russia). To do this, the corresponding powders with the stoichiometric molar ratio TiC:Ti:Al = 2:1:1 were mixed and pressed into cylindrical granules with a diameter and height of \approx 12 mm, which were immersed into molten KCl–NaCl salt (molar ratio 1/1) and kept in the muffle furnace at 1300 °C for 3 h in an air atmosphere. The resulting powders were washed with deionized water until the salts were completely removed, filtered, and dried at 100 °C.

Hydrofluoric acid (HF, 49 wt.%, Russian Standard 10484-78, Russia) was used for the selective etching of aluminum layers from Ti_3AlC_2 MAX phase to create layered $Ti_3C_2T_x$ MXene titanium carbides. For this, 100 mL of HF solution (25 wt%) was poured into a Teflon reactor, into which 5 g of the Ti_3AlC_2 MAX phase powder was then immersed in small portions. The reaction was carried out at 30 °C for 60 h with constant stirring. The resulting suspension was washed several times with HCl (6 M) and then with deionized water until neutral pH \approx 6 was reached, and then it was dried in the vacuum oven at 60 °C for 24 h.

(b) Electrodeposition of nickel–Ti₃C₂T_x composite coatings

Composite Ni–Ti₃C₂T_x MXene coatings were deposited on a steel substrate (steel 45) from a sulfate–chloride bath (Table 1).

Table 1. Electrolyte composition and deposition parameters used for Ni–Ti₃C₂T_x MXene.

Electrolyte Composition	Concentration, g/L	Deposition Parameters
NiSO ₄ ·7H ₂ O	220	Temperature <i>t</i> = 45 °C, pH ≈ 4.5
NiCl ₂ ·6H ₂ O	40	Constant stirring
CH ₃ COONa	30	Cathode current densities
Ti ₃ C ₂ T _x MXene	1	<i>i</i> _c = 7, 8, 9, 10 A/dm ²

Ti₃C₂T_x MXene was added into the bath in the form of a powder. Electrochemical deposits of pure nickel were obtained from the above-mentioned solution without Ti₃C₂T_x. The thickness of all studied coatings was 20 µm. Pretreatment of the electrode surface consisted of mechanical cleaning by sandpaper from 200 to 2500 grit systematically, anodic etching in 48% H₃PO₄ with Pb counter electrode, and washing in distilled water.

(c) Investigation of structure and properties

The phase composition was studied with the help of ARL X'TRA device (Thermo Scientific, Ecublens, Switzerland) applying Cu K α radiation (λ = 0.15412 nm). Ti₃C₂T_x powders morphology and the surfaces of the nickel coatings were examined using an ASPEX Explorer scanning electron microscope (ASPEX, Framingham, MA, USA).

Electrochemical measurements were performed on a P-30J potentiostat (Elins, Russia). The potentials were set relative to a saturated silver chloride reference electrode and recalculated on the hydrogen scale.

Vickers microhardness (HV) was measured using a PMT-3 instrument (AO LOMO, Russia). A tetrahedral diamond pyramid was statically pressed into the Ni electrolytic deposits under a load of 100 g. The average penetration depth of the imprint was 3.06 µm. The distance between the imprints was no more than two diagonals. Based on the tests conducted, values of both diagonals of the imprint were determined. The calculation of HV was carried out according to the data of seven parallel measurements. The experiment error was 3%.

To assess the corrosion–electrochemical behavior of nickel coatings, anodic potentiodynamic plots were obtained in the 0.5 M H₂SO₄ solution (potential sweep rate *V*_p = 8 mV/s). Corrosion rate was studied in 3.5% NaCl solution.

3. Results and Discussion

The properties of CECs significantly depend on the properties and structure of the dispersed particles. Figure 1 shows the X-ray diffraction patterns (XRD) of the Ti₃AlC₂ MAX phase powder obtained by sintering in the melt of salts and Ti₃C₂T_x MXene powder synthesized by the selective etching of Al from the MAX phase structure. The phase composition of the initial powder used for etching is represented by Ti₃AlC₂ (JCPDS 52-0875) as the main phase, and a small content of the secondary phase Ti₂AlC. After the MAX phase powder treatment in the HF solution, significant changes are observed in the diffraction pattern. All the peaks corresponding to the Ti₃AlC₂ phase disappear and wide peaks appear at angles 2θ = 7.78° and 2θ = 15°, which confirm its transformation into a multilayer Ti₃C₂T_x MXene. In this case, the peak obtained upon reflection from the (002) plane shifted towards smaller angles from 2θ = 9.47° to 2θ = 8.91°. Thus, it is possible to draw the conclusion that the lattice parameter *c* increased due to the destruction of Ti–Al bonds and an etching of the Al layer from the Ti₃AlC₂ structure.

The study of Ti₃AlC₂ powders using scanning electron microscopy (SEM) after their treatment in hydrofluoric acid shows that their morphology is represented by layered accordion-like particles (Figure 2a,b). This indicates that the Al layers were successfully

etched from the MAX phase with hydrofluoric acid, resulting in a layered 2D $\text{Ti}_3\text{C}_2\text{T}_x$ MXene structure.

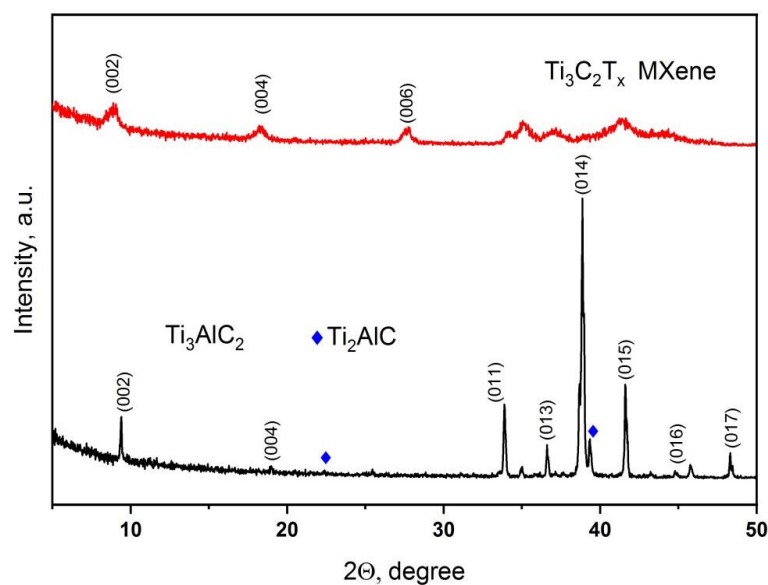


Figure 1. XRD patterns of Ti_3AlC_2 MAX phase and $\text{Ti}_3\text{C}_2\text{T}_x$ MXene.

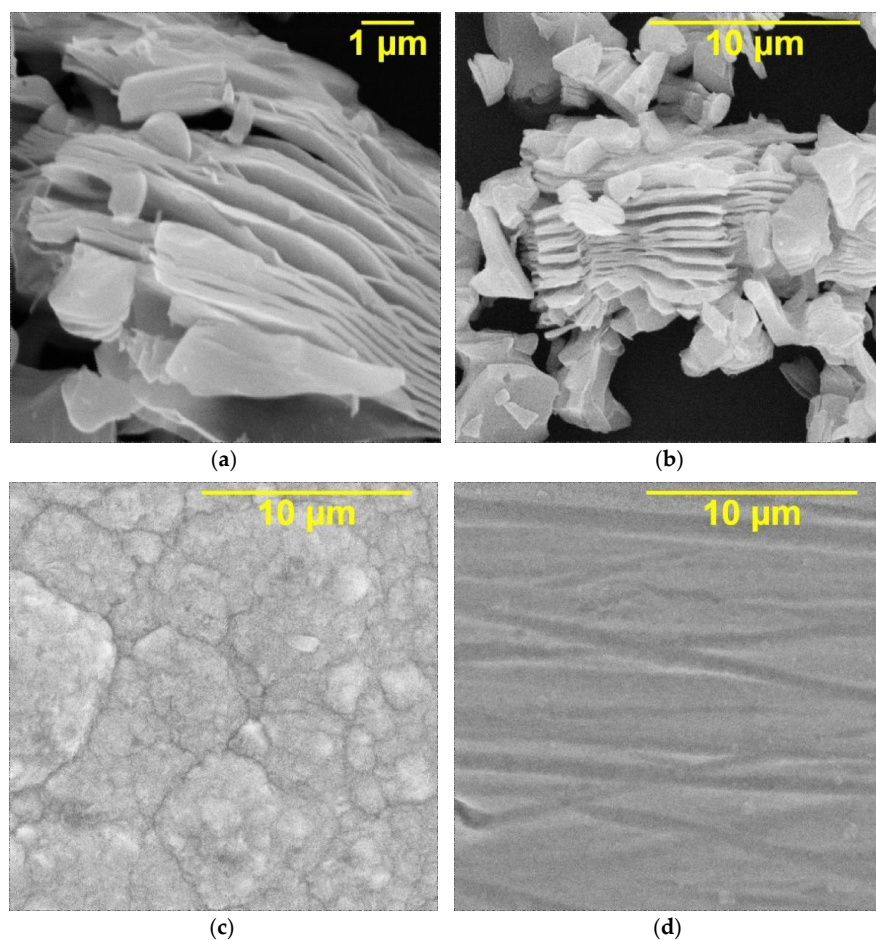


Figure 2. SEM images of $\text{Ti}_3\text{C}_2\text{T}_x$ MXene (a,b), pure Ni (c), and CEC Ni- $\text{Ti}_3\text{C}_2\text{T}_x$ MXene (d) deposited at $i_c = 10 \text{ A/dm}^2$.

The study of the process of the joint electrodeposition of nickel with $\text{Ti}_3\text{C}_2\text{T}_x$ MXene by taking potentiodynamic plots (PDP) shows that the inclusion of the $\text{Ti}_3\text{C}_2\text{T}_x$ dispersed phase into the nickel-plating electrolyte affects the kinetics of electrode processes. A nickel deposit in the presence of dispersed particles is formed on the cathode at less negative electrode potentials. Electrodeposition currents of nickel– $\text{Ti}_3\text{C}_2\text{T}_x$ MXene CECs increase compared with pure nickel (Figure 3), which indicates an increase in the rate of the cathodic process. During electrodeposition, Ni ions in the electrolyte with a positive charge are absorbed by $\text{Ti}_3\text{C}_2\text{T}_x$ particles due to electrostatic forces. Nickel cations with adsorbed particles move towards the cathode and reduce on the electrode surface, forming a nickel deposit together with the dispersed phase. The $\text{Ti}_3\text{C}_2\text{T}_x$ MXene compound (Figure 2a,b) has a developed multilayer structure with a large specific surface area, which provides more vacant places for nucleation. This increases the rate of nucleation and the deposition rate of the nickel matrix as a whole. The higher the nucleation rate, the more metal grains are formed on the surface, which must determine the fine grain size of the electrochemical deposits. The SEM study of the surface of nickel coatings shows that the dispersed phase of $\text{Ti}_3\text{C}_2\text{T}_x$ MXene significantly changes the morphology of nickel deposits. The $\text{Ti}_3\text{C}_2\text{T}_x$ layers prevent excessive nickel grain growth and promote the formation of a fine-grained, uniform deposit, which is consistent with the analysis of coating morphology using the SEM method (Figure 2c,d). Under the influence of $\text{Ti}_3\text{C}_2\text{T}_x$, there occurs a transition from an amorphous, coarse-grained, and disordered structure of pure nickel (Figure 2c) to a fine-grained, uniform, and dense structure of the composite coating (Figure 2d).

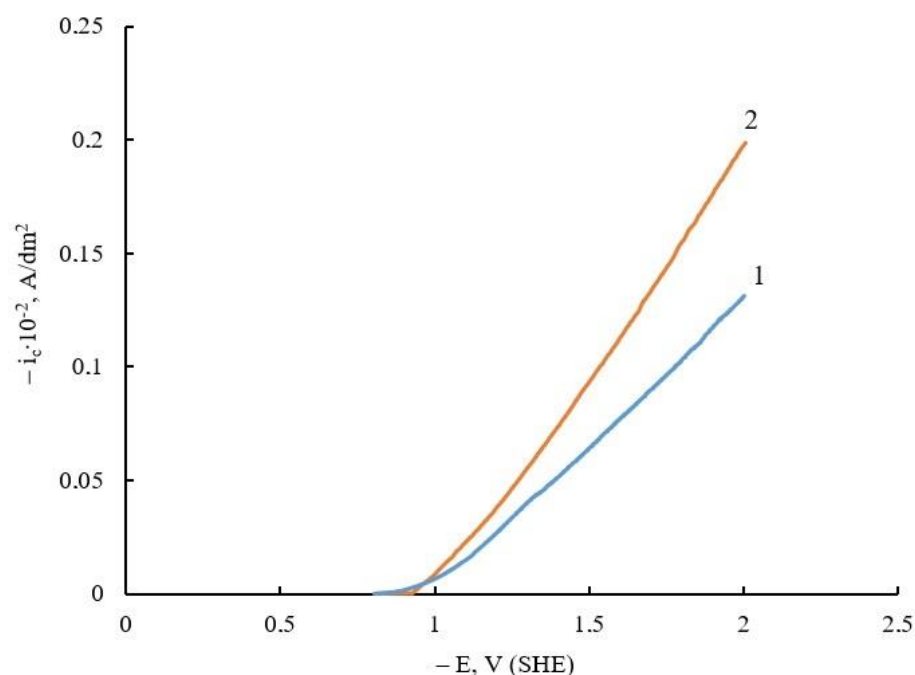


Figure 3. Potentiodynamic plots of Ni electrodeposition process (1) and Ni– $\text{Ti}_3\text{C}_2\text{T}_x$ MXene CEC (2) (potential sweep rate $V_p = 10$ mV/s).

Nickel forms a face-centered cubic lattice, which corresponds to the peaks at 44° and 52° in the diffractogram (Figure 4). When nickel is modified with the $\text{Ti}_3\text{C}_2\text{T}_x$ MXene compound, the intensities of the peaks at 44° and 52° , which correspond to the nickel (111) and (200) planes, increase significantly compared with pure nickel. This indicates a change in the crystal structure under the influence of the dispersed phase—the growth of a nickel crystal occurs simultaneously in two directions (111) and (200), and the peak corresponding to the crystal plane (200) is predominant for the nickel– $\text{Ti}_3\text{C}_2\text{T}_x$ CEC, while for pure nickel, according to Figure 4, the preferred crystal growth orientation is the (111) plane. The appearance of the peaks corresponding to Ti and C in the nickel– $\text{Ti}_3\text{C}_2\text{T}_x$ CEC diffraction

pattern proves the inclusion of $\text{Ti}_3\text{C}_2\text{T}_x$ into the metal matrix of the electrochemical coating. The peaks corresponding to Ni in the XRD pattern of the Ni coatings increase significantly. The intensity ratio of the composite coating changes because $\text{Ti}_3\text{C}_2\text{T}_x$ has a layered structure. Nickel deposits and grows on the Mxene sheets, which leads to changes in the crystallite structure and, hence, to an increase in the peaks (the Mxene sheets affect the crystal growth).

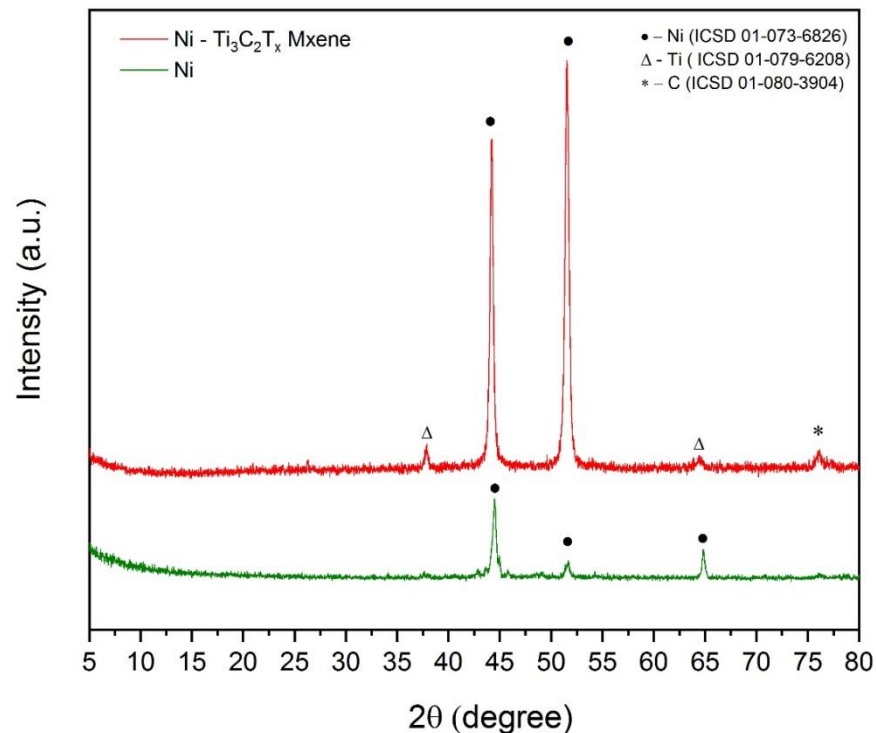


Figure 4. XRD patterns of Ni coating and CEC Ni- $\text{Ti}_3\text{C}_2\text{T}_x$ MXene deposited at $i_c = 10 \text{ A/dm}^2$.

The penetration of a dispersed phase into the structure of an electrochemical metal matrix leads to a shift, not only in their composition and structure, but also in their operational properties. Of significant practical interest are the physical and mechanical characteristics of metal surfaces, in particular their microhardness. With an increase in the cathode current density, the microhardness of the researched nickel coatings grows (Table 2). This is probably due to the inclusion of hydrogen and hydroxides in their structure, which leads to the distortion and compression of crystallites. On the transition from Ni coatings without a disperse phase to Ni- $\text{Ti}_3\text{C}_2\text{T}_x$ CECs, there is a growth in microhardness of about 1.80 times in the investigated interval of current densities (Table 2). This effect is due to several reasons. First, this is due to the formation of a fine-grained structure and the dispersion strengthening of the nickel matrix in the presence of $\text{Ti}_3\text{C}_2\text{T}_x$. The embedded $\text{Ti}_3\text{C}_2\text{T}_x$ sheets are located between the forming nickel grains, preventing their growth and, thus, ensuring the grinding of the grains of the composite coatings. The small grain size increases the length of the grain boundaries and prevents the movement of defects (primarily dislocations) along the crystal lattice. Secondly, the excellent physical-mechanical properties of the $\text{Ti}_3\text{C}_2\text{T}_x$ particles also contribute to an increase in the hardness of the studied CECs. Moreover, the embedded particles are distributed along the grain boundaries and act as a barrier to the propagation of slip planes.

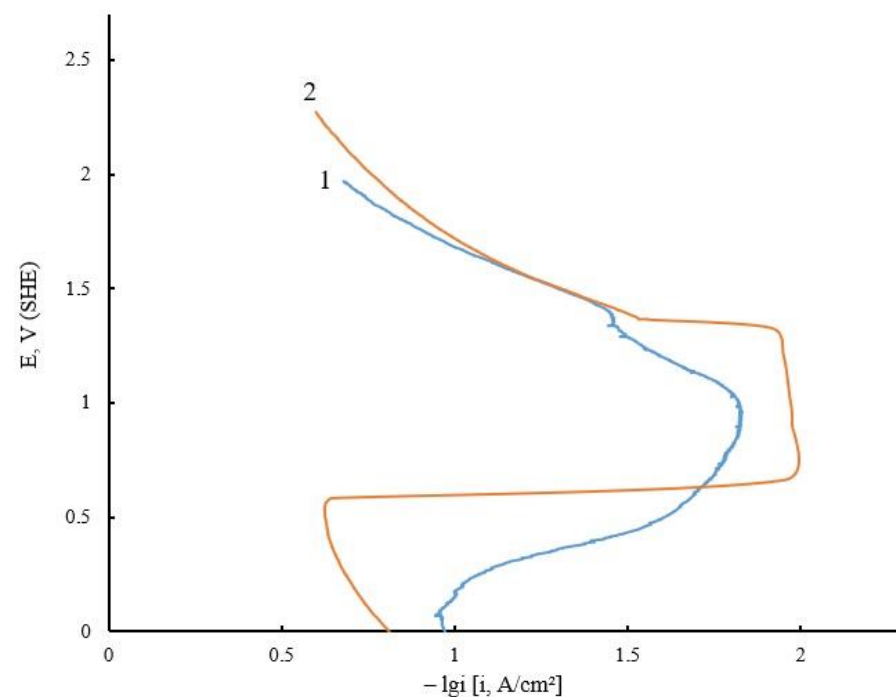
Table 2. Microhardness $HV_{0.10}$ values in MPa of Ni coatings *.

Cathode Current Density i_c , A/dm ²	Ni	Ni-Ti ₃ C ₂ T _x
7	1938	3563
8	2150	3894
9	2350	4189
10	2459	4565

* Microhardness of steel substrate (steel 45) is 894 MPa.

Another important property of electrochemical deposits is corrosion resistance. The following aspects are relevant to this problem: increasing the reliability of metal products to reduce material losses and prevent industrial accidents, as well as the preservation of the world's metal resources. When metal comes into contact with an electrolyte solution, electrochemical corrosion occurs, which is a combination of two conjugate heterogeneous processes: the anodic oxidation of the metal and the cathodic reduction of the oxidizer. In the case of composite coatings, the nature of corrosion damage is conditioned by both the characteristics of the metal matrix and the dispersed phase.

The corrosion–electrochemical behavior of the Ni deposits was investigated in 0.5 M H₂SO₄ solution using the chronovoltamperometry method. The anodic PDPs of Ni and the Ni-Ti₃C₂T_x MXene CEC (Figure 5) show that the particles of the disperse phase increase the potential and, accordingly, decrease the active anodic dissolution current of the studied coatings. The potential for the beginning of the passivation of pure Ni and CEC Ni-Ti₃C₂T_x are close. A characteristic feature of the anodic PDP of the Ni-Ti₃C₂T_x CEC is a wide, pronounced passive area, while for a Ni deposit not containing an MXene disperse phase, it is significantly smoothed. It should be noted that the rate of metal dissolution does not depend much on the potential value and can only decrease slightly when the potential shifts to the more positive values. Consequently, the broadening of the passive region for the composite coating is associated with the influence of the MXene dispersed phase. On the basis of chronovoltamperometry studies in 0.5 M H₂SO₄ solution, it was expected the corrosion rate of the Ni-Ti₃C₂T_x CECs to be less than that of the Ni deposits without a disperse phase.

**Figure 5.** Potentiodynamic polarization plots of Ni (1) and Ni-Ti₃C₂T_x MXene (2) (deposited at $i_c = 10$ A/dm²) in 0.5 M H₂SO₄.

The corrosion rate of the nickel-based electrolytic deposits was measured using the weight loss, when kept in 3.5% NaCl for 24 h (the templates were weighed before and after dipping), with the help of the next equation [34,35]:

$$\text{Corrosion rate} = \frac{K W}{A T D}$$

where K is constant ($8.76 \cdot 10^4$), W is the mass loss in g, A is the exposed area of a coating template (1 cm^2), T is the dipping time in hours, and D is the density of nickel (8.90 g/cm^3).

Tests in 3.5% NaCl medium show that the corrosion rate of Ni–Ti₃C₂T_x deposits decreases by 1.60–1.75 times in comparison with that of electrolytic Ni without MXene (Table 3). It is difficult to single out only one reason for this effect. When analyzing the influence of Ti₃C₂T_x on the corrosion behavior of the studied Ni coatings, it is worth paying attention to several factors. The Ni–Ti₃C₂T_x coatings have a regular fine-grained structure, in contrast to Ni without an MXene phase (Figure 2c,d), which conditioned a uniform distribution of the corrosion current over the surface. Wetting the coating surface with a corrosive medium is important. A fine-grained metal surface is more difficult to wet, which results in a slower corrosion rate. It should be noted that corrosion is a spontaneous process with a Gibbs free energy negative value. The tendency of nickel to suffer corrosion damage depends on the crystallographic orientation, which conditions the surface free energy per unit area of the material. The ability of metal ions to penetrate through the cross-section of the dispersed particles in the coating affects the corrosion behavior. The high impermeability and stability of the Ti₃C₂T_x MXene phase contribute to the lengthening of the diffusion path for an aggressive environment and prevents the penetration of Ni²⁺ ions through the micro-particle cross section. The effect of the dispersed phase in the matrices of CECs is observed only if the particles form compounds that are more resistant to corrosion than the metal deposit at the phase boundaries or throughout the volume. Obviously, compounds like that are also formed in the volume of the studied composite coatings. All the above-mentioned reasons working in common determined a decrease in the corrosion rate of Ni–Ti₃C₂T_x CECs compared with electrolytic Ni without MXene.

Table 3. Corrosion rates in mm/year of nickel coatings *.

Cathode Current Density i_c , A/dm ²	Ni	Ni–Ti ₃ C ₂ T _x
7	0.656	0.410
8	0.574	0.328
9	0.451	0.287
10	0.328	0.205

* Corrosion rate of steel substrate (steel 45) is 0.881 mm/year.

4. Conclusions

In this work we synthesized Ti₃C₂T_x MXene powder and studied its structure. The conducted electrochemical research allows us to conclude that in the galvanostatic electrolysis mode, CECs are formed from the sulfate–chloride nickel plating bath including Ti₃C₂T_x MXene particles. The addition of Ti₃C₂T_x MXene into the nickel matrix leads to a transformation in the microstructure and has a remarkable effect on the physicomechanical properties and corrosion rate of obtained CECs. The modification of electrolytic Ni by the Ti₃C₂T_x MXene results in a growth in the microhardness of coatings by about 1.80 times, and their corrosion rate decreases by 1.60–1.75 times. These effects are due to the formation of a fine-grained structure and the strengthening of the nickel matrix by adding Ti₃C₂T_x particles. The Ni–Ti₃C₂T_x MXene CEC obtained at $i_c = 10 \text{ A/dm}^2$ has better operating characteristics.

Author Contributions: Conceptualization, V.T.; data curation, D.T. and A.D.; formal analysis, A.T. (Alexey Tsyganov), N.G. and A.T. (Alena Tribis); investigation, V.T., A.T. (Alena Tribis), D.T., A.D., A.T. (Alexey Tsyganov) and N.G.; methodology, V.T., A.D., D.T., A.T. (Alexey Tsyganov) and N.G.; project administration, V.T.; supervision, V.T., A.D. and A.T. (Alexey Tsyganov); visualization, A.D., A.T. (Alena Tribis), D.T., A.T. (Alexey Tsyganov) and M.L.; writing—original draft, V.T., A.D. and A.T. (Alexey Tsyganov); writing—review and editing, V.T., A.D., A.T. (Alena Tribis), D.T., A.T. (Alexey Tsyganov), N.G. and M.L. All authors participated in the discussion of the results and the writing of the text of the article. All authors have read and agreed to the published version of the manuscript.

Funding: Funding: A.T. (Alexey Tsyganov) and N.G. thank for the synthesis, SEM and XRD of MXene the Russian Science Foundation, grant number 19-73-10133, <https://rscf.ru/en/project/19-73-10133/> (accessed on 3 August 2022).

Institutional Review Board Statement: Not applicable.

Informed Consent Statement: Not applicable.

Data Availability Statement: Not applicable.

Conflicts of Interest: The authors declare no conflict of financial or non-financial interest requiring disclosure in this article.

Abbreviations

The list of acronyms:

CEC	composite electrochemical coating
PDP	potentiodynamic plot
SEM	scanning electron microscopy
XRD	X-ray diffraction

References

- Orinakova, R.; Turonova, A.; Kladekova, D.; Galova, M.; Smith, R.M. Recent developments in the electrodeposition of nickel and some nickel-based alloys. *J. Appl. Electrochem.* **2006**, *36*, 957–972. [\[CrossRef\]](#)
- Dordsheikh Torkamani, A.; Velashjerdi, M.; Abbas, A.; Bolourchi, M.; Maji, P. Electrodeposition of nickel matrix composite coatings via various boride particles: A review. *J. Compos. Compd.* **2021**, *3*, 106–113. [\[CrossRef\]](#)
- Tseluikin, V.N. Composite coatings modified with nanoparticles: Structure and properties. *Nanotechnologies Russ.* **2014**, *9*, 1–14. [\[CrossRef\]](#)
- Huang, P.C.; Hou, K.H.; Hong, J.J.; Lin, M.H.; Wang, G.L. Study of fabrication and wear properties of Ni–SiC composite coatings on A356 aluminum alloy. *Wear* **2021**, *477*, 203772. [\[CrossRef\]](#)
- Xiang, Y.; He, Y.; Tang, W.; Li, H.; Zhang, Y.; Song, R.; Liu, B.; He, Y.; Guo, X.; He, Z. Fabrication of robust Ni-based TiO₂ composite@TTOS superhydrophobic coating for wear resistance and anti-corrosion. *Colloids Surf.* **2021**, *629*, 127394. [\[CrossRef\]](#)
- Iacovetta, D.; Tam, J.; Erb, U. Synthesis, structure, and properties of superhydrophobic nickel–PTFE nanocomposite coatings made by electrodeposition. *Surf. Coat. Technol.* **2015**, *279*, 134–141. [\[CrossRef\]](#)
- Tseluikin, V.N.; Chubenko, I.S.; Gun'kin, I.F.; Pankst'yanov, A.Y. Colloidal dispersion of fullerene C60 free of organic solvents. *Russ. J. Appl. Chem.* **2006**, *79*, 325–326. [\[CrossRef\]](#)
- Tseluikin, V.N.; Solov'ova, N.D.; Gun'kin, I.F. Electrodeposition of nickel–fullerene C60 composition coatings. *Prot. Met.* **2007**, *43*, 388–390. [\[CrossRef\]](#)
- Yang, P.; Wang, N.; Zhang, J.; Lei, Y.; Shu, B. Investigation of the microstructure and tribological properties of CNTs/Ni composites prepared by electrodeposition. *Mater. Res. Express* **2022**, *9*, 036404. [\[CrossRef\]](#)
- Tseluikin, V.N.; Koreshkova, A.A. Electrochemical deposition and properties of composite coatings consisting of zinc and carbon nanotubes. *Russ. J. Appl. Chem.* **2015**, *88*, 272–274. [\[CrossRef\]](#)
- Tseluikin, V.N.; Koreshkova, A.A. Pulsed electrodeposition of composite coatings based on zinc–nickel alloy. *Prot. Met. Phys. Chem. Surf.* **2018**, *54*, 453–456. [\[CrossRef\]](#)
- Hong, Q.; Wang, D.; Yin, S. The microstructure, wear and electrochemical properties of electrodeposited Ni–diamond composite coatings: Effect of diamond concentration. *Mater. Today Commun.* **2023**, *34*, 105476. [\[CrossRef\]](#)
- Yasin, G.; Arif, M.; Nizam, N.M.; Shakeel, M.; Khan, M.A.; Khan, W.Q.; Hassan, T.M.; Abbas, Z.; Farahbakhsh, I.; Zuo, Y. Effect of surfactant concentration in electrolyte on the fabrication and properties of nickel–graphene nanocomposite coating synthesized by electrochemical co-deposition. *RSC Adv.* **2018**, *8*, 20039–20047. [\[CrossRef\]](#)
- Jyotheender, K.S.; Srivastava, C. Ni–graphene oxide composite coatings: Optimum graphene oxide for enhanced corrosion resistance. *Compos. Part B* **2019**, *175*, 107145. [\[CrossRef\]](#)

15. Lou, G.; Shen, L.; Qian, Y.; Chen, Y.; Bai, H.; Cheng, H.; Xu, J.; Yang, Y. Study on the antibacterial and anti-corrosion properties of Ni-GO/Ni-rGO composite coating on manganese steel. *Surf. Coat. Technol.* **2021**, *424*, 127681. [\[CrossRef\]](#)
16. Naguib, M.; Kurtoglu, M.; Presser, V.; Lu, J.; Niu, J.; Heon, M.; Hultman, L.; Gogotsi, Y.; Barsoum, M.W. Two-dimensional nanocrystals produced by exfoliation of Ti_3AlC_2 . *Adv. Mater.* **2011**, *23*, 4248–4253. [\[CrossRef\]](#) [\[PubMed\]](#)
17. Wang, Y.; Zhang, M.; Xu, W.; Shen, X.; Gao, F.; Zhu, J.; Wan, X.; Lian, X.; Xu, J.; Tong, Y. Chemical Preparation of New $\text{Ti}_3\text{C}_2\text{MXene}$ and the Performance and Mechanism of Memristor Based on MXene. *Acta Phys. Chim. Sin.* **2022**, *38*, 1907076.
18. Huang, Y.; Wang, C.; Wang, R.; Zhang, Y.; Li, D.; Zhu, H.; Wang, G.; Zhang, X. Ethanol Solution Plasma Loads Carbon Dots onto 2D HfNb_3O_8 for Enhanced Photocatalysis. *ACS Appl. Mater. Interfaces* **2023**, *15*, 1157–1166. [\[CrossRef\]](#)
19. Cheng, S.; Xiong, Q.; Zhao, C.; Yang, X. Synergism of 1D CdS/2D Modified $\text{Ti}_3\text{C}_2\text{Tx}$ MXene Heterojunctions for Boosted Photocatalytic Hydrogen Production. *Chin. J. Struct. Chem.* **2022**, *41*, 2208058–2208064.
20. Chang, C.; Chen, W.; Chen, Y.; Chen, Y.; Chen, Y.; Feng, D.; Fan, C.; Fan, H.J.; Fan, Z.; Gong, C.; et al. Recent progress on Two-Dimensional Materials. *Acta Phys. Chim. Sin.* **2021**, *37*, 2108017. [\[CrossRef\]](#)
21. Cao, X.; Hou, C.; Li, Y.; Li, K.; Zhang, Q.; Wang, H. MXenes-Based Functional Fibers and Their Applications in the Intelligent Wearable Field. *Acta Phys. Chim. Sin.* **2022**, *38*, 2204058. [\[CrossRef\]](#)
22. Bu, F.; Zagho, M.M.; Ibrahim, Y.; Ma, B.; Elzatahry, A.; Zhao, D. Porous MXenes: Synthesis, structures, and applications. *Nano Today* **2020**, *30*, 100803. [\[CrossRef\]](#)
23. Naguib, M.; Barsoum, M.W.; Gogotsi, Y. Ten Years of Progress in the Synthesis and Development of MXenes. *Adv. Mater.* **2021**, *33*, 2103393. [\[CrossRef\]](#) [\[PubMed\]](#)
24. Salim, O.; Mahmoud, K.A.; Pant, K.K.; Joshi, R.K. Introduction to MXenes: Synthesis and characteristics. *Mater. Today Chem.* **2019**, *14*, 100191. [\[CrossRef\]](#)
25. Ronchi, R.M.; Arantes, J.T.; Santos, S.F. Synthesis, structure, properties and applications of MXenes: Current status and perspectives. *Ceram. Int.* **2019**, *45*, 18167–18188. [\[CrossRef\]](#)
26. Li, X.; Wang, C.; Cao, Y.; Wang, G. Functional Mxene Materials: Progress of Their Applications. *Chem. Asian J.* **2018**, *13*, 2742. [\[CrossRef\]](#)
27. Rosenkranz, A.; Righi, M.C.; Sumant, A.V.; Anasori, B.; Mochalin, V.N. Perspectives of 2D MXene Tribology. *Adv. Mater.* **2023**, *35*, 2207757. [\[CrossRef\]](#)
28. Miao, X.; Li, Z.; Liu, S.; Wang, J.; Yang, S. MXenes in tribology: Current status and perspectives. *Adv. Powder Mater.* **2023**, *2*, 100092. [\[CrossRef\]](#)
29. Bian, H.; Du, Y.; Ren, Y.; Wu, H.; Ma, Y.; Yang, B.; Tang, S.; Bin, D.; Lu, H.; Meng, X. One-step electrodeposition of polypyrrole/ $\text{Ti}_3\text{C}_2\text{Tx}$ MXene composite coating for 304SS bipolar plates in PEMFC. *Surf. Coat. Technol.* **2023**, *462*, 129460. [\[CrossRef\]](#)
30. Du, Y.; Wang, D.; Si, P.; Wei, L.; Wang, Y.; Yu, B.; Zhang, X.; Ye, S. Electrodeposition of a Ni-P- $\text{Ti}_3\text{C}_2\text{Tx}$ /MoS₂ coating incorporating MoS₂ intercalated $\text{Ti}_3\text{C}_2\text{Tx}$ particles. *Surf. Coat. Technol.* **2018**, *354*, 119–125. [\[CrossRef\]](#)
31. Zhang, L.; Huang, S.; Weng, Y.; Li, J.; Han, P.; Ye, S.; Zhang, X. Preparation of Ni-P- $\text{Ti}_3\text{C}_2\text{Tx}$ -Ce composite coating with enhanced wear resistance and electrochemical corrosion behavior on the surface of low manganese steel. *Surf. Coat. Technol.* **2022**, *441*, 128508. [\[CrossRef\]](#)
32. Liu, Y.; Fan, B.; Xu, B.; Yang, B. Ambient-stable polyethyleneimine functionalized $\text{Ti}_3\text{C}_2\text{Tx}$ nanohybrid corrosion inhibitor for copper in alkaline electrolyte. *Mater. Lett.* **2023**, *337*, 133979. [\[CrossRef\]](#)
33. Galvin, T.; Hyatt, N.C.; Rainforth, W.M.; Reaney, I.M.; Shepherd, D. Molten salt synthesis of MAX phases in the Ti-Al-C system. *J. Eur. Ceram. Soc.* **2018**, *38*, 4585–4589. [\[CrossRef\]](#)
34. Yang, F.; Kang, H.; Guo, E.; Li, R.; Chen, Z.; Zeng, Y. The role of nickel in mechanical performance and corrosion behaviour of nickel-aluminium bronze in 3.5 wt.% NaCl solution. *Corros. Sci.* **2018**, *139*, 333–345. [\[CrossRef\]](#)
35. Rekha, M.Y.; Srivastava, C. Microstructural evolution and corrosion behavior of Zn-Ni-graphene oxide composite coatings. *Met. Mater. Trans. A* **2019**, *50*, 5896–5913. [\[CrossRef\]](#)

Disclaimer/Publisher's Note: The statements, opinions and data contained in all publications are solely those of the individual author(s) and contributor(s) and not of MDPI and/or the editor(s). MDPI and/or the editor(s) disclaim responsibility for any injury to people or property resulting from any ideas, methods, instructions or products referred to in the content.